

SHEAR CARRYING CAPACITY OF REINFORCED CONCRETE BEAMS WITH VARIOUS A/D RATIOS DAMAGED DUE TO THE ALKALI-SILICA REACTION

TOMOHIRO MIKI^{*}, TOMOHIRO ARAKAWA[†] AND YOHEI KOSHIBA[†]

^{*} Kobe University, Department of Civil Engineering
1-1 Rokkodai, Nada, Kobe 657-8501, Japan
e-mail: mikitomo@port.kobe-u.ac.jp

[†] Kobe University, Department of Civil Engineering
1-1 Rokkodai, Nada, Kobe 657-8501, Japan

Key words: ASR, RC beams, shear carrying capacity, diagonal cracks, image analysis

Abstract: This study presents experimental investigations on the shear carrying capacity of RC beams in which alkaline silica reaction (ASR) of the concrete has occurred. In the experiments, RC beams with shear span effective depth ratio, $a/d = 1.0, 2.5$ and 4.5 were prepared. Before conducting a loading test, visual observation and measurements of the crack and crack width were conducted using a digital microscope to quantitatively evaluate the degree of damage caused by the cracks due to the ASR. In the shear loading test, the initiation and propagation of the diagonal cracks were measured by image analysis, and simultaneously rebar strain and concrete strain were measured to calculate the neutral axis in the beam section. The experiments show that the effects of a/d ratio on the shear strength of the RC beams with different durations of outdoor exposure can be clarified based on the difference in the angle and propagation of the diagonal cracks.

1 INTRODUCTION

In the maintenance management system for existing reinforced concrete (RC) structures, it is necessary to appropriately evaluate the residual performance of the deteriorated RC structure, in particular, the load capacity and deformation performance to perform a rational maintenance cycle. Among the deterioration of the concrete structures, in the RC member in which the alkali-silica reaction (ASR) has occurred, the concrete cracks when the expansion due to the ASR becomes extremely large. It is revealed that in RC beams where such damage has occurred, the presence of cracks in concrete changes not only the mechanical properties of concrete but also the adhesion properties between rebar and concrete, resulting in changes in shear resistance mechanism. However, the degree of influence of each has not been understood

quantitatively. There is research for example on the residual shear resistance of RC members without reinforcement numerically (Saouma et al. 2016) and full scale cantilever slabs without shear reinforcement (Schmidt et al. 2014), respectively, which were subjected to the ASR.

This study presents experiment to evaluate the shear carrying capacity of RC beams damaged by the ASR with various durations of outdoor exposure. The specimens used in this research were the three series of ASR damaged RC beams and sound RC beams as a reference with ratios of shear span to effective depth, a/d of $1.0, 2.5$ and 4.5 , respectively. In the experimental investigation, in order to extensively investigate the damage of each RC beam quantitatively, the crack was observed in detail before conducting a loading test. As for the shear carrying mechanism of the RC

Table 1: Mix proportion of the concrete

G_{\max} mm	Slump cm	W/C %	Air %	s/a %	kg/m ³							
					W	C	S_n	S_r	G_n	G_r	NaCl	AE water redu. agent
20	18	63	5	48	181	287	422	432	466	475	12.4	575 ml

S_n : no-reactive fine aggregate, S_r : reactive fine aggregate,
 G_n : no-reactive aggregate, G_r : reactive aggregate

beams damaged due to the ASR, the crack propagation which was caused by ASR and the progress of cracking that occurred during the loading of RC beams were particularly discussed.

2 EXPERIMENTAL PROCEDURES

2.1 Outlines of specimens

Table 1 shows the mix proportion of the concrete used. Ordinary portland cement for cement and AE water reducing agent for admixture were used. The maximum size of cause aggregate is 20 mm. Both fine and coarse aggregates were mixed where the ratio of reactive and nonresponsive aggregates in the volume of 1:1 that was decided as a pessimum content. Each specimen was made by the same concrete mix

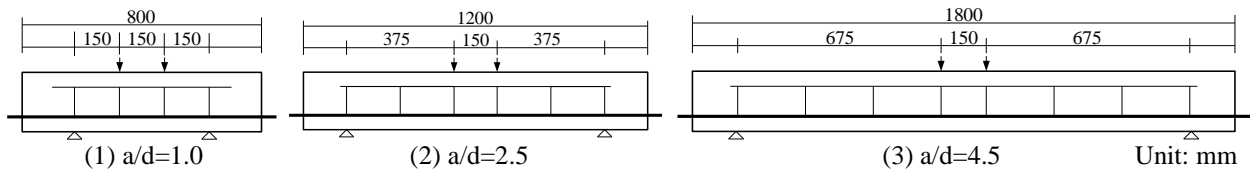
In order to compare with a specimen using this concrete mix (referred as “ASR” specimen hereafter), a sound specimen (“N” specimen) is used as a reference specimen, in which a mix proportion with all reactive coarse and fine aggregates were substituted with non-

reactive aggregate. In order to accelerate the ASR, a predetermined amount of NaCl was added at the time of mixing, but it was not used in the N specimens.

The specimens were a rectangular cross-sectional RC beams with a cross-sectional height of 200 mm, the width of 150 mm, an effective height of 150 mm, and a length of 800 mm, 1200 mm, or 1800 mm, respectively. The specimen name indicates different a/d ratios, such as ASR1.0, ASR2.5, ASR4.5 for ASR specimens and N1.0, N2.5, N4.5 for N specimens, respectively.

Figure 1 shows the dimension of the beam and the arrangement of reinforcing bars. High strength steel bar D22 (nominal yield strength 930 N/mm²) was used for tensile rebars, and SD 295A-D6 (measured yield strength 338 N/mm²) was used for stirrups and assembled rebars.

The ASR specimens were exposed outdoors with the tensile side upward. The exposure period of each series is shown in **Table 2**. Hereafter, for example, as in ASR 1.0-1, the series number indicating the exposure period is

**Figure 1:** Specimens.**Table 2:** Mechanical properties of concrete

Series	Cylindrical comp. strength (N/mm ²)	Splitting tensile strength (N/mm ²)	Elastic Modulus (N/mm ²)	Age or exposure periods
N	37.1	3.62	28500	1 year
ASR-1	25.6	2.48	11500	2 years 10 months
ASR-2	27.2	---	5670	3 years
ASR-3	34.0	2.14	6630	3 years 5 months
ASR-4	30.6	1.94	9280	5 years 5 months

written at the end of each specimen name. In this experiment, twelve ASR specimens were used totally for a series of 4 exposure periods, among three samples of a/d , and 1 for each of N specimens.

It has been confirmed that an expansion which has been measured by using reference prism specimens of $100 \times 100 \times 200$ mm was around 1200μ or more for the series of the ASR-1.

2.2 Mechanical Properties of Materials

Cylindrical specimens of 100 mm diameter and 200 mm height were prepared with the same mix proportion for ASR specimens and exposed under the same condition as the RC beams. The mechanical properties of concrete were tested at the same day as the loading test of RC beams. The results are indicated as an average value of 3 specimens for each. The experimental results are summarized in **Table 2**. From these results, it can be seen that the compressive strength of the ASR specimens varies with the age of the material but is slightly smaller than that of the sound specimens. On the other hand, compared with the compressive strength, the decrease of the tensile strength and the elastic modulus of the ASR-damaged concrete is remarkably smaller compared to the sound one. In particular, it is considered that the decrease in the elastic modulus is caused by the large compressive deformation under the external load due to the

effect of cracking by the ASR in the cylindrical specimen subjected to compression.

2.3 Loading tests of RC beams

In the loading test, 4-point bending loading was performed using a 2000 kN universal testing machine. The loading rate was approximately 0.2 kN/sec. Measurements were load, displacement at the loading points and supports, opening displacement of crack, and rebar strain, respectively. During the loading test, the crack propagation was visually observed and the crack width was measure crack scaling. In addition, the side of the specimen was photographed with a digital camera at each load level, and the strain distribution of the concrete was calculated by image analysis. The tensile rebars were fixed using anchor plates and nuts at the end of the RC beam to prevent slippage at the rebar anchorage area. The strain gauges attached to the rebar and the rebar strain was recorded at certain intervals. In the ASR specimens, a crack displacement gauge was installed at a part of the ASR cracks generated along the tensile rebar, and the opening displacement of the cracks was measured.

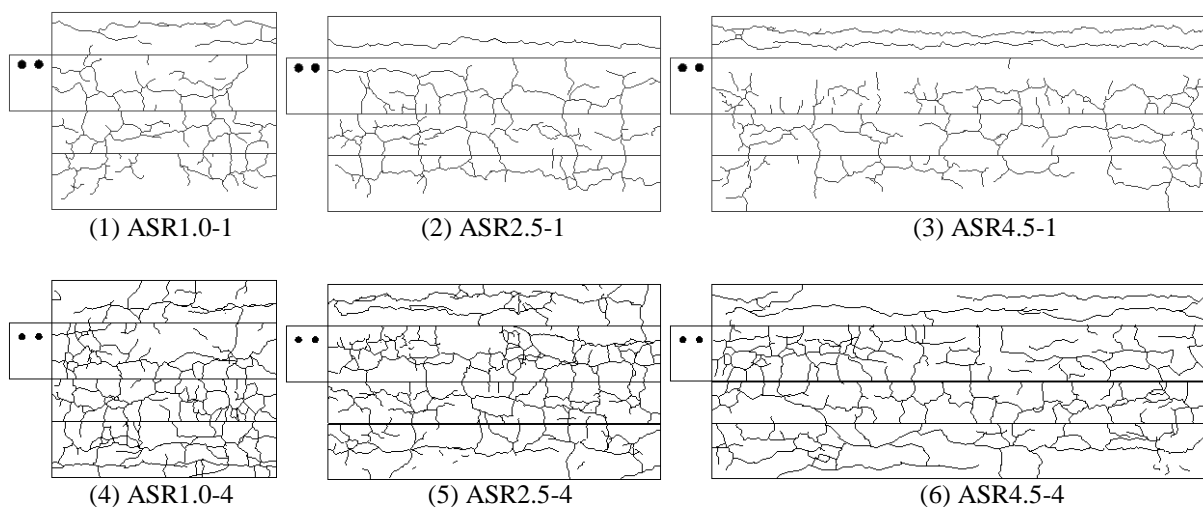


Figure 2: Crack distribution in for ASR specimens (ASR-1, ASR-4)

3 DAMAGE CONDITION OF RC BEMAS DUE TO ASR

3.1 Visual observation of cracks

Figure 2 shows sketches of the cracks observed on the surface of the ASR specimen for the ASR-1 and ASR-4 series, respectively. The sketch in the figure from the top indicates the bottom of the RC beam, the side 1, the top and the side 2, respectively. From these sketched figures, it can be seen that cracks occurred significantly along the axial direction of the tensile rebars. On the other hand, in the upper surface of the RC beam (the compression side in loading), the cracks were meshed and mapped irregularly. This is caused due to a fact that expansion due to ASR was not constrained by the rebars. However,

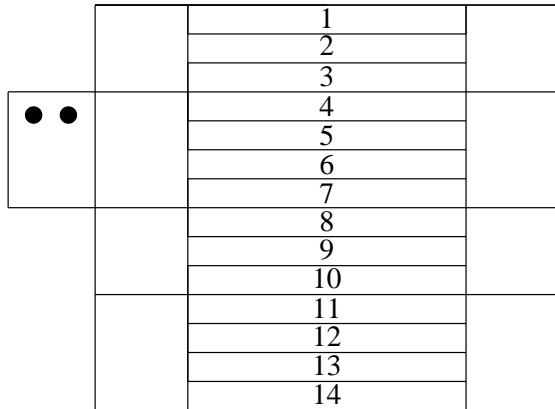


Figure 3: Location and classification of the surface of the RC beam to measure the ASR cracks

although the exposure period and the material age were different, there was no significant difference in the crack condition. The reason may be that after the exposure starts, cracks were generated by expansion due to ASR, while the crack width increased after the initiation of cracks, therefore, the cracks were not initiated in the period of following exposure.

Crack length density, average crack width, and crack cross-sectional area density were measured and calculated as the indexes to quantitatively evaluate the damage degree by the ASR. The value was calculated in the location and classification of the surface of the RC beam as shown in Figure 3. For the member axis direction, the measurement of cracks was conducted in the domain between the supports in the loading test. The surface of the beam was classified into the bottom surface (sections 1 to 3), the side surface 1 (sections 4 to 7), the top surface (sections 8 to 10), and the side surface 2 (sections 11 to 14), respectively. In each section, the crack length was measured from a line segment using a sketch of the crack in the ASR specimen. In addition, the crack width was measured at a point in a square grid of 50 mm as the largest crack width in each grid which was identified using a digital microscope in the minimum range of around 10 μm. The average value of

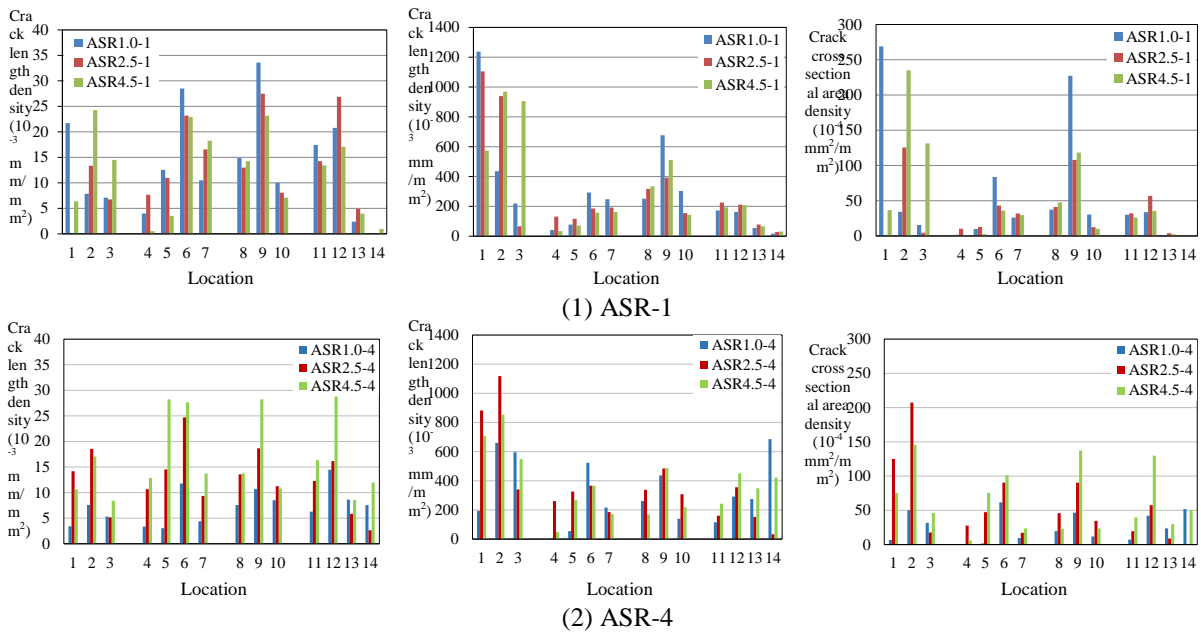


Figure 4: Crack density, crack width and crack cross-sectional area density for ASR specimens (ASR-1, ASR-4)

the crack width in all sections was calculated, and finally, the crack cross-sectional area density was determined by dividing the product of the crack length in each section and the average value of the crack width by the cross-sectional area of the section.

The measured results are summarized in **Figure 4**. From this figure, it can be seen that the crack length density, the average crack width, and the crack cross-sectional area density showed large values at the sections of 2, 6, 9, 12 and 13. This indicates that the height center of the side surface of the ASR specimens is more cracked than the upper and lower ends. This is considered to be due to the fact that the central part of the side is not much constrained by reinforcement. Moreover, in the vicinity of the tensile bars, large cracks occurred along the tensile bar, and it is found that the average crack width is large in the sections of 1, 2 and 3.

3.2 Initial deformation of RC beam due to expansion by ASR

As a result of ASR expansion, an initial deformation was observed that was convex upward on the beam. In order to measure the amount of deformation, as shown in **Figure 5**, the amounts of deformation d_1 and d_2 in the direction perpendicular to the axis of the fulcrum and the loading point on the bottom were measured. In the ASR-1 series, the deformations were 0.45 mm and 0.30 mm for $a/d = 1.0$ beam, and were 0.94 mm, 0.53 mm and 3.86 for $a/d = 2.5$ and 4.5 beams, respectively. This initial deformation is in the opposite direction to the displacement in the loading test, and is relatively large, about 30% to 40% of the displacement at maximum load. It should be noted that the influence of this initial deformation on the deformation that occurs when receiving an external load in the loading test cannot be ignored.

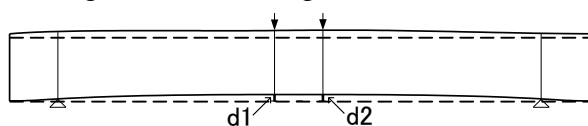


Figure 5: Initial deformation due to ASR

4 RESULTS AND DISCUSSION

4.1 Load-displacement relationships

Figure 6 shows the load-displacement relationship. It can be seen that the maximum load is greater in the ASR specimens of all a/d ratios than in the N specimens. However, in the $a/d = 1.0$ and 4.5 cases, the capacity of the ASR specimens increases about 25% compared to one of the N specimens, while in the $a/d = 2.5$ case, a slight difference of the capacity was observed. There was no significant difference in the initial stiffness comparing the N and ASR specimens.

Comparing the series ASR-1 and ASR-4 with different exposure periods, it can be seen that the difference in the behavior of the RC beams of ASR-1 and ASR-4 is relatively small in the cases of a/d ratio = 2.5. In the experiment of the beams with $a/d = 1.0$ or 4.5, however, the maximum load of ASR specimen showed significantly larger as compared to that of the N specimen. This result shows a different trend since the compressive strength of the ASR specimen using cylindrical specimens indicates lower than that of the N specimen. This is caused by cracking caused by the ASR, bond deterioration of reinforcing bars, initial deformation due to an internal expansion pressure, and consequently these facts may influence the shear resistance mechanism of RC beams. In addition, the crack pattern of the ASR specimen has indicated that the cracks due to the ASR occurred both along the axial direction of the tensile bars and irregularly occurred on the compression side. In the following sections, image analysis is performed from digital images taken during loading, and in particular, the progress of the crack is further discussed.

4.2 Crack propagation

Crack pattern after the loading test is shown in **Figure 7**. In the N specimen, it can be seen in the figure that the diagonal cracks occurred to connect between a loading point and support when the RC beam reached the maximum load. On the other hand, in the ASR specimen, it is found that the multiple diagonal

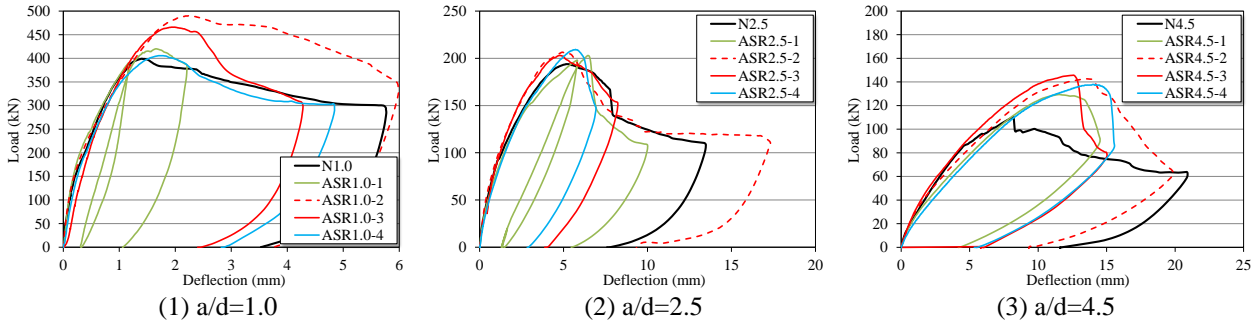


Figure 6: Load and mid-span deflection relationships

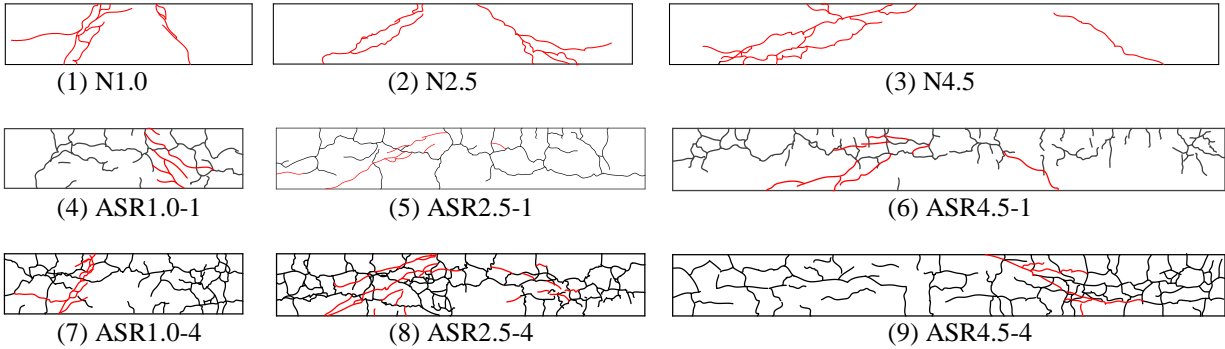


Figure 7: Crack patterns in RC beams (red line; cracks under loading, black line; ASR induced cracks)

cracks in the shear span which was generated to connect the cracks due to the ASR that occurred before loading occurred under the external loading. In the loading test, the load resisting by the ASR-damaged RC beam decreased ultimately with the opening of the crack.

The angle of diagonal crack at the ultimate stage of ASR specimen with $a/d = 1.0$ was steeper as compared to the ASR specimens with different a/d ratios, and it seems that there was slight influence of the existing cracks on the propagation of diagonal cracks. On the other hand, as for the ASR specimen with a/d

$= 4.5$, it can be seen that the angle of the diagonal crack was relatively small and affected by the ASR-induced cracks which have been developed in the horizontal direction. In this specimen, the diagonal cracks tend to be influenced by existing cracks, and consequently resulted in different failure mode in shear for the damaged RC beam.

4.3 Principal strain distribution

Image analysis was conducted by using digital photos which were taken for RC beams during loading tests. Figure 8 shows the target domains of image analysis for ASR1.0 and

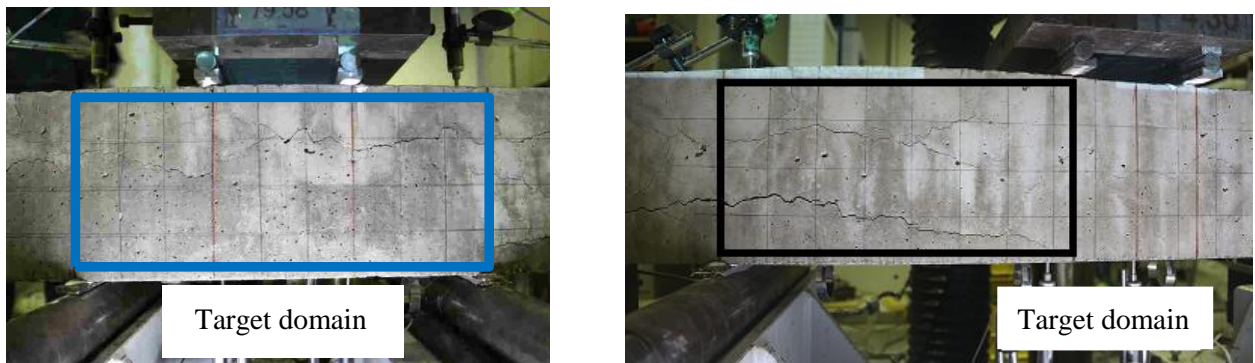


Figure 8: Target domain of image analysis (right: $a/d = 1.0$, left: $a/d = 2.5$)

ASR2.5 specimens as an example of the strain measurement of the concrete surface and its distribution. The target domain of image analysis is set as a whole range of both shear and bending spans for the RC beams with $a/d = 1.0$ specimen, while as a range of shear span failed at the ultimate stage for the RC beams with $a/d = 2.5$ and 4.5 .

Figure 9 to 11 show the principle strain distribution of the RC beams obtained by the image analysis. In these figures, the contour represents the magnitude of strain, indicating in the order of blue, green, yellow and red colors in which the displayed distortion ranges from 0 of the strain in blue, 0.05 of the strain in red. The strain measured is shown that at

loads of flexural cracking, diagonal cracking and near the ultimate stage. Here, the principle strain distributions at the similar load level and maximum load are shown so that the crack initiation and propagation in the ASR specimens and the N specimens can be compared.

As comparing the specimens with different a/d ratios, it is found that the load at the initiation of bending cracking of the ASR specimen is similar to the N specimen. It can be seen in the figure of the principal strain distribution at 150 kN for the specimen with $a/d = 1.0$, 70 kN for $a/d = 2.5$, and 50 kN for $a/d = 4.5$ that tensile strain is shown and localized vertically directing upward from the

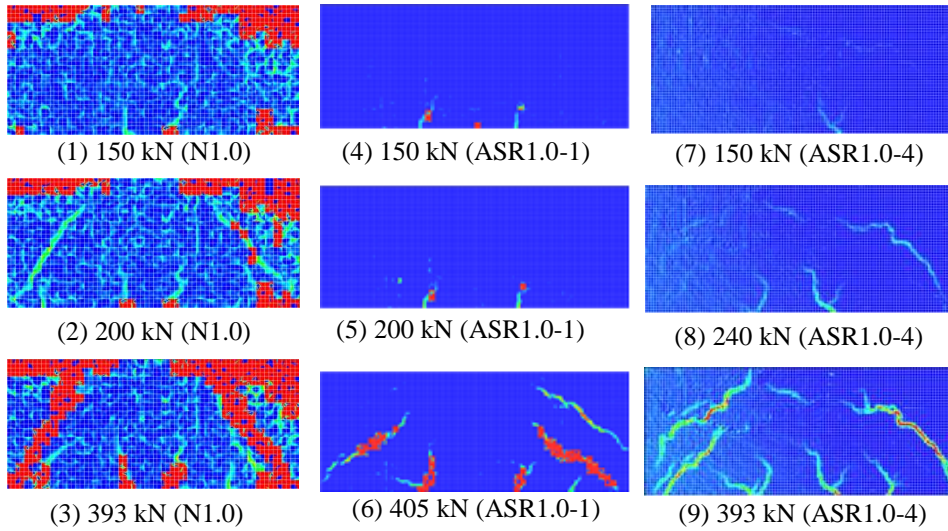


Figure 9: Principle strain distribution in the both shear and bending spans ($a/d = 1.0$)

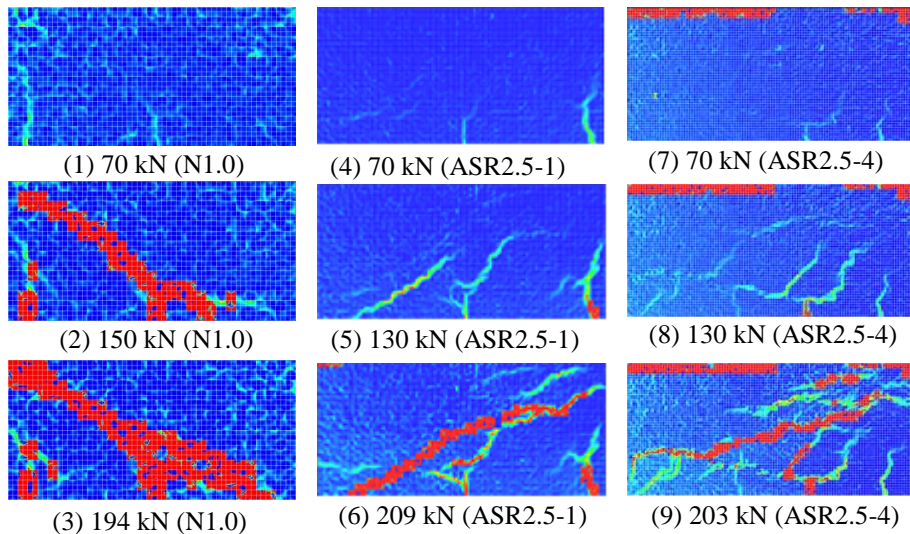


Figure 10: Principle strain distribution in the failed shear span ($a/d = 2.5$)

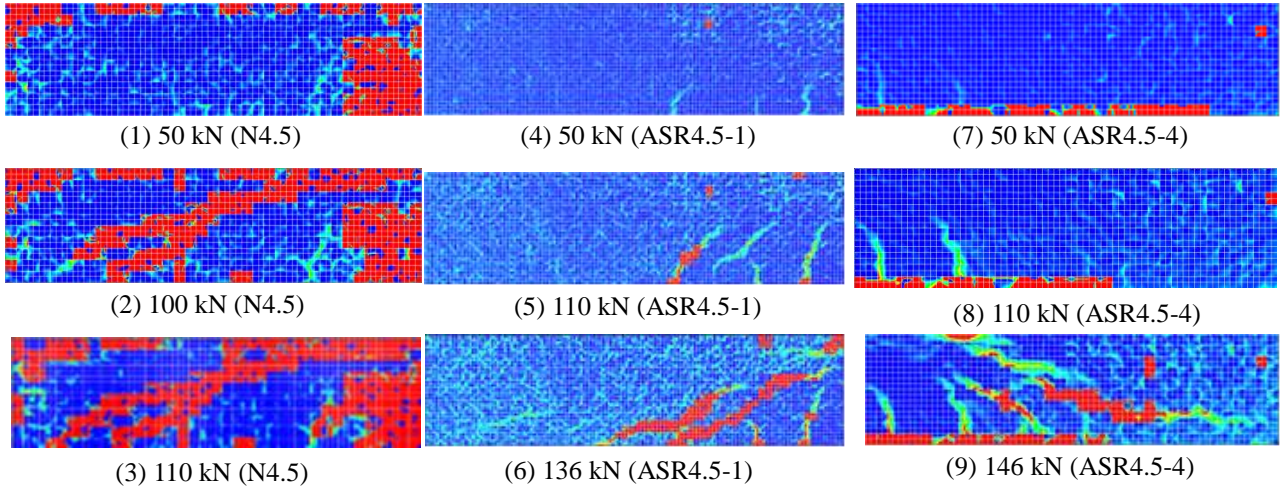


Figure 11: Principle strain distribution in the failed shear span ($a/d = 4.5$)

bottom of the beam. From the results of the concrete cylindrical specimens, the difference in tensile strength between the N and the ASR specimens is as small as 0.2 N/mm^2 , which may not affect the occurrence of bending cracks.

However, after the bending cracking, the progress of tensile strain differs between the ASR and N specimens. The principal strain in tension has progressed to about the all height in the N specimen, while about half the height in the ASR specimen.

In particular, comparison in **Figures 9 and 11** (1), (4) and (7) shows that the bending cracks in the N specimens with $a/d = 1.0$ and $a/d = 4.5$ reaches two thirds of the height, while that in the ASR specimens reaches about one third of the height. This delay of the development of the principle strain may be because the chemical prestressing remaining internally by the ASR expansion but it releases the tensile stress in the concrete after bending cracking.

Figures 9 to 11 (2), (5) and (8) show the principal strain distribution when the diagonal crack develops in the N and the ASR specimens. It is found that in the case of $a/d = 1.0$ and 4.5 the diagonal cracks have already occurred in the N specimen at this loading level, while that has not yet occurred in the ASR specimen. On the other hand, in the case of $a/d = 2.5$, the diagonal cracks similarly occurred in both the N and ASR specimens. This result yields that the increase in the load

of the initiation of diagonal cracking results in the increase in the shear capacity.

Looking at figures of (3), (6) and (9) in **Figures 9 to 11** as a result at the maximum load, in the N specimen the large strain in tension is concentrated along with the diagonal crack that occurred connecting from the support to the loading point. In the case of the ASR specimens, it can be seen that although multiple diagonal cracks occurred in the diagonal direction in the shear span, one dominant diagonal crack which was similar location and direction to that in the N specimen occurred at the ultimate stage.

It is obvious that the image analysis in this study reveals that in the ASR specimens with $a/d = 1.0$ and 4.5 , the initiation and distribution of diagonal cracks differed from that in the N specimens. In addition, in the case of $a/d = 2.5$, the ASR specimen showed similar shear carrying capacity to that of the sound specimen. However, it seems reasonable to conclude that it is needed to discuss further on the mechanism of an increase in the shear carrying capacity in the case of deep beams and slender beams that is significantly damaged due to the ASR.

5 CONCLUSIONS

In this study, investigation on cracks due to the ASR which was reproduced by outdoor exposure for RC beams with different a/d ratios was conducted. In addition, loading tests was carried out to experimentally investigate

the shear carrying capacity of RC beams damaged by the ASR. The conclusions obtained in this study are shown as follows.

- 1) Loading tests were conducted on ASR specimens and sound beams with different exposure periods. The initial gradients of the load-displacement relationships of the ASR specimens with $a/d = 1.0$ and 4.5 were similar to those of the sound specimens, while its shear capacity was larger than that of the sound specimens.
- 2) Image analysis can capture the initiation and propagation of crack under the external loading in the sound and ASR specimen. However, it is needed to discuss further on the mechanism of an increase in the shear carrying capacity in the cases of deep beams and slender beams that are significantly damaged due to the ASR.

9th International Conference on Fracture Mechanics of Concrete and Concrete Structures **9**:1-7

ACKNOWLEDGEMENTS

This research was partially supported from the Japan Society for the Promotion of Science (JSPS) regarding Fund for the Promotion of Joint International Research (JSPE KAKENHI Grant Number 15KK0208).

REFERENCES

- [1] Saouma, V.E., Hariri-Ardebili, M.A., Pape, Y.L., and Balajia, B. 2016. Effect of alkali-silica reaction on the shear strength of reinforced concrete structural members. A numerical and statistical study *Nuclear Engineering and Design* **310**: 295-310
- [2] Schmidt, J.W., Hansen, S.G., Barbosa, R.A., and Henriksen, A. 2014. Novel shear capacity testing of ASR damaged full scale concrete bridge *Engineering Structures* **79**: 365-374
- [3] Miki, T., Matsutani, K. and Miyagawa, Y., 2013. Evaluation of crack propagation in ASR damaged concrete based on image analysis, *Proceedings of 8th International Conference on Fracture Mechanics of Concrete and Concrete Structures* **8**: 1787-1794
- [4] Miki, T., and Tsukahara, H. 2016. Crack propagation in ASR damaged concrete detected by image analysis *Proceedings of*